Influence of the type of intercalation on spin-glass formation in the Fe-doped TaS_2 (Se_2) polytype family

A. S. Ovchinnikov [1,2] I. G. Bostrem,[1] Vl. E. Sinitsyn [1] N. M. Nosova [1] and N. V. Baranov[1,2]

[1]*Institute of Natural Science and Mathematics, Ural Federal University, Ekaterinburg 620002, Russia*
[2]*Institute of Metal Physics, Ural Division, Russian Academy of Sciences, Ekaterinburg 620219, Russia*

We suggest an explanation based on the Blume-Capel model of why some layered compounds of the iron-intercalated transition metal dichalcogenides $TaS_2(Se_2)$ exhibit spin-glass behavior, while another group of this family demonstrates low-temperature paramagnetism. In these materials, the doped Fe atoms either substitute the Ta atoms with losing their magnetic moments or sit between the $TaS_2(Se_2)$ layers keeping their spin states. The Blume-Capel model allows us to introduce a chemical potential to control a balance of the intercalated elements of both types. The Ghatak-Sherrington theory of spin-glass behavior of this model predicts an existence of a tricritical point that means that there is a concentration threshold of Fe ions retaining their magnetic moments, above which spin-glass ordering occurs. Below the threshold, Fe ions behave as independent paramagnetic centers. We build temperature dependencies of magnetic susceptibility and field dependencies of magnetization to highlight specific features of the model related with a variable content of Fe ions in the high-spin state. A specific crystal structure of the layered transition metal dichalcogenides gives an opportunity to increase the concentration of ions with nonzero magnetic moments by co-intercalating non-Kramers $3d$ ions into the van der Waals gaps. This process may trigger spin-glass ordering in the initially paramagnetic Fe-doped $TaS_2(Se_2)$ polytype complexes.

I. INTRODUCTION

Synthesis, optical, electrical, and magnetic properties of three-dimensional (3D) layered transition metal dichalcogenides have been extensively studied for several decades [1,2]. The development of modern synthetic methods and experimental techniques makes it possible to study and use the monolayers of these compounds [3,4]. Recent achievements in this field have restarted the interest in intercalation as a powerful and effective method of doping two-dimensional materials starkly modifying their physical properties [5].

The $3d$ transition metal dichalcogenides TX_2 consist of the transition metal (T) elements which are sandwiched between two layers of chalcogen atoms ($X =$ S, Se, or Te). The covalent bonding within the TX_2 layers is strong, while the bonding between the layers is ensured by rather weak van der Waals (vdW) interaction between the chalcogen atoms [6]. The specific crystal structures of these materials arise from both the local environment of the T ions within TX_2 (trigonal-prismatic or octahedral coordination) and the different ways of stacking the TX_2 sandwiches [7]. Insertion of foreign species (organic and organometallic molecules, alkali and alkali earth metals, $3d$ transition metals) into the vdW gap opens the possibility to obtain intercalated complexes, whose properties may differ significantly from those of the parent compounds [8].

The first-row transition metal intercalates M_xTX_2 ($M =$ V, Cr, Mn, Fe, Co, Ni) are of particular interest because, at certain concentrations (mostly, at $x \geqslant 0.20$), localized moments present on the ordered superlattices of $3d$ intercalate ions may show a variety of types of magnetic ordering [9,10]. However, at small concentrations of the $3d$ ions, many of the

three-dimensional dichalcogenides of transition metals exhibit a spin-glass or cluster-glass behavior [11–15].

The iron-intercalated TiS_2 and $TiSe_2$ are examples of M_xTX_2 materials, in which spin-glass effects are manifested fairly clearly [16–21]. The spin-glass behavior is attributed to the presence of disordered interstitial Fe^{2+} ions coupled via an oscillatory RKKY exchange mechanism. The increase of the Fe concentrations gives rise to a plethora of different kinds of long-range magnetic order [22–24].

In contrast to titanium complexes, where intercalation occurs due to insertion of Fe ions into the vdW gap only, the situation is not so unambiguous for $TaS_2(Se_2)$ [25–30], in which the Fe ions may be randomly distributed either on Ta sites or between the $TaS_2(Se_2)$ layers (Fig. 1). In particular, a spin-glass behavior was revealed in some polytypes, namely, $2H$-Fe_xTaSe_2 (although this is disputed in Ref. [26]) and $4Hb$-Fe_xTaS_2; however, their counterparts, $2H$-Fe_xTaS_2 and $4Hb$-Fe_xTaSe_2, do not show local-moment formation [27]. The difference may be related to (i) different orbital states of conduction electrons, $3d$ in Ti atoms and $5d$ in Ta atoms, which mediate RKKY interaction between the local moments of Fe^{2+} ions [31]; (ii) the competition between the crystal-field splitting of the $3d$ states of Fe atoms and their intra-atomic exchange coupling [9] that governs local-moment formation. Obviously, the appearance of a spin-glass state depends on the local crystal-field interaction which dictates whether the intercalated iron atoms lose or retain their magnetic moments.

Traditionally, spin-glass phenomena in transition-metal dichalcogenides are explained in terms of theories with a fixed number of doped intercalant elements. However, this interpretation begs the question of why those parts of Fe ions,
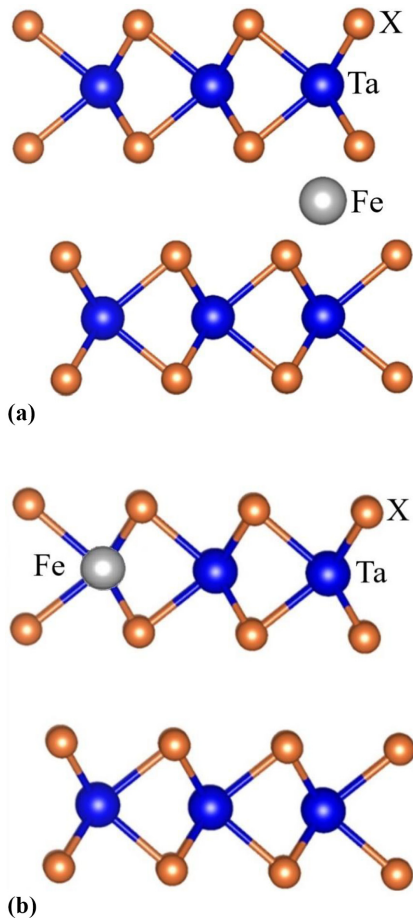
FIG. 1. Types of Fe intercalation into the TaX_2 (X = S, Se) layered system: (a) insertion; (b) substitution.

which are inserted between the TaS$_2$(Se$_2$) layers in nonmagnetic materials and retain their magnetic moments, do not form their own spin-glass order, but, instead, behave as a set of independent impurities, whose susceptibility follows a Curie law. More generally, what is a reason behind separation into nonmagnetic and spin-glass systems in the Fe-doped TaS$_2$(Se$_2$) polytype family?

In our study, we address these issues within the framework of the Blume-Capel (BC) model, which has been actively treated in the mean-field approximation in the 1960s [32,33]. Its generalization for spin glasses was first given by Ghatak and Sherrington (GS) [34]. We suggest interpreting a term of the BC-model Hamiltonian, which was attributed to crystal-field splitting in the GS theory, to the action of a chemical potential, which governs a balance of the intercalated Fe ions with or without magnetic moment. This approach is close to that of the Blume-Emery-Griffiths model proposed to describe phase separation in liquid He^3 − He^4 mixtures [35].

The characteristic feature of the BC model is the occurrence of the first-order phase transition. In the GS theory, it is manifest as a tricritical point, in which a line of second-order spin-glass transitions breaks when crystal-field splitting exceeds a threshold value and "low-temperature paramagnetism" (singlet state) arises. In our case, it means that there is a threshold in the content of the intercalated Fe ions retaining their moments, above which spin-glass ordering is favored.

This might explain the experimentally observed division of the TaS$_2$(Se$_2$) complexes into nonmagnetic with embedded paramagnetic impurities and spin-glass systems.

In our analysis we introduce a random site-dependent chemical potential with a Gaussian distribution whose mean may be interpreted as a chemical potential regulating the balance between those Fe ions that lose their magnetic moments and those that retain them. The width of the distribution takes into account nonstoichiometric effects, which have an influence on the crystal-field splitting in Fe^{2+} ions located at different crystallographic positions. We demonstrate that increase of the width diminishes the concentration threshold of Fe ions in the high-spin state, at which spin-glass behavior becomes possible. As well, we discuss a way to shift the distribution center by adding the non-Kramers 3d ions (for example, Cr^{3+}, Mn^{2+}, Co^{2+}) into the vdW gaps. Their co-intercalation may trigger a spin-glass behavior in the initially nonmagnetic Fe-doped TaS$_2$(Se$_2$) compounds that would provide evidence of validity of the BC model for the family of tantalum disulphide (diselenide) polytype complexes.

The paper is organized as follows. In Sec. II, we give key facts about the BC spin-glass model treated in the replica-symmetric (RS) approximation, about stability of the RS solutions, and appropriate phase diagrams of spin-glass behavior. We discuss an influence of the random Weiss fields on the spin-glass ordering in the same section. Temperature dependence of magnetic susceptibility and field dependence of magnetization curves are given in Sec. III. As well, consideration of the co-intercalation effects is reported here. Finally, our summary and conclusions are presented in Sec. IV.

II. THE MODEL

A. Replica-symmetric solutions

The Blume-Capel model of the randomly distributed Fe ions in the presence of an external magnetic field is defined by the Hamiltonian

$$\mathcal{H} = -\sum_{(ij)} J_{ij} S_i S_j - \sum_i h_i S_i - \sum_i \Delta_i S_i^2, \qquad (1)$$

where $S_i = 0$ stands for the ions losing their magnetic moments in the low-spin state, and $S_i = \pm 1$ corresponds to the ions retaining their moments in the high-spin state. Here, $i = 1, 2, \ldots, N$ and the first sum runs over all pairs of spins. The on-site potential Δ_i dictates whether the low-spin state lies lower in energy than the high-spin state ($\Delta_i < 0$), or vice versa ($\Delta_i > 0$).

The couplings J_{ij}, acting between all pairs, the random fields h_i, and the on-site potentials Δ_i are considered as quenched random variables with Gaussian probability distributions

$$P(J_{ij}) = \sqrt{\frac{N}{2\pi J^2}} \exp\left[-\frac{N}{2J^2}\left(J_{ij} - \frac{J_0}{N}\right)^2\right], \qquad (2)$$

$$P(h_i) = \frac{1}{\sqrt{2\pi\sigma_h^2}} \exp\left[-\frac{1}{2\sigma_h^2}(h_i - h_0)^2\right], \qquad (3)$$

$$P(\Delta_i) = \frac{1}{\sqrt{2\pi\sigma_\Delta^2}} \exp\left[-\frac{1}{2\sigma_\Delta^2}(\Delta_i - \Delta_0)^2\right]. \qquad (4)$$

The shift J_0 of the exchange distribution with the standard deviation $J/\sqrt{N}$ may be due to an emergence of a prevailing distance between the intercalated Fe ions. The mean Δ_0 plays the role of a chemical potential, which governs a number of those ions, which retain their magnetic moments in positions between the $TaS_2(Se_2)$ layers. The width σ_Δ comprises nonstoichiometric effects, which have an influence on the crystal-field splitting in Fe^{2+} ions located at different crystallographic positions. The appearance of random magnetic fields h_i may be attributed to the possibility of configuring nearest-neighbor clusters of the doped ions. Obviously, in the absence of the external magnetic field h_0, the random fields are centered around zero with the variance σ_h^2.

The free energy of the system for a given realization of the disorder is averaged by means of these distributions,

$$
[F(\{J_{ij}\}, \{h_i\}, \{\Delta_i\})]_{J,h,\Delta}
$$
$$
= \int \prod_{(ij)} [dJ_{ij} P(J_{ij})] \int \prod_i [dh_i P(h_i)]
$$
$$
\times \int \prod_i [d\Delta_i P(\Delta_i)] F(\{J_{ij}\}, \{h_i\}, \{\Delta_i\}), \quad (5)
$$

where $F = -(1/\beta) \ln Z$ on the right-hand side of this equation, and Z is the partition function of the model.

Using the replica trick, the free energy per spin may be presented as

$$
f = -\lim_{N\to\infty} \lim_{n\to 0} \frac{1}{nN\beta} ([Z^n]_{J,h,\Delta} - 1). \quad (6)
$$

In this way, we have for the partition function of a replicated system after performing the average over J_{ij}, h_i and Δ_i,

$$
[Z^n]_{J,h,\Delta} = \sum_{\{S_i^a\}} \exp \left[\frac{\beta J_0}{N} \sum_{(ij)} \sum_a S_i^a S_j^a \right.
$$
$$
+ \frac{\beta^2 J^2}{2N} \sum_{(ij)} \left(\sum_a S_i^a S_j^a \right)^2 + \beta h_0 \sum_{ia} S_i^a
$$
$$
+ \beta \Delta_0 \sum_{ia} (S_i^a)^2 + \frac{\beta^2 \sigma_h^2}{2} \sum_i \left(\sum_a S_i^a \right)^2
$$
$$
\left. + \frac{\beta^2 \sigma_\Delta^2}{2} \sum_i \left(\sum_a (S_i^a)^2 \right)^2 \right], \quad (7)
$$

where a is a replica index ($a = 1, \ldots, n$).

Using the Hubbard-Stratonovich transformations to linearize the quadratic terms in (7), we obtain (see Supplemental Material [36])

$$
[Z^n]_{J,h,\Delta} = \int \left(\prod_a dm_a \right) \int \left(\prod_{(ab)} dq_{ab} \right) \int \left(\prod_a d\mu_a \right)
$$
$$
\times \exp [\mathcal{L}(\{m_a\}, \{q_{ab}\}, \{\mu_a\})]. \quad (8)
$$

Here, the effective Lagrangian is given by

$$
\mathcal{L}(\{m_a\}, \{q_{ab}\}, \{\mu_a\})
$$
$$
= -\frac{N\beta J_0}{2} \sum_a m_a^2 - \frac{N\beta^2 J^2}{2} \sum_{(ab)} q_{ab}^2 - \frac{N\beta^2 J^2}{4} \sum_a \mu_a^2
$$
$$
+ N \ln \left[\sum_{\{S^a\}} \exp [\mathcal{H}_{\text{eff}}(\{S^a\})] \right], \quad (9)
$$

where a set of auxiliary variables m_a, q_{ab}, and μ_a is introduced. The indices a, b are replica labels and $\sum_{(ab)}$ denotes a sum over distinct pairs of replicas.

In the effective Hamiltonian of replica interactions

$$
\mathcal{H}_{\text{eff}}(\{S^a\}) = \sum_a F_S^a S^a + \sum_{(ab)} F_Q^{ab} S^a S^b
$$
$$
+ \sum_a F_N^a (S^a)^2 + \sum_{(ab)} F_{Q^2}^{ab} (S^a S^b)^2 \quad (10)
$$

the coupling constants and fields are defined as

$$
F_S^a = \beta (J_0 m_a + h_0), \quad (11)
$$

$$
F_Q^{ab} = \beta^2 (J^2 q_{ab} + \sigma_h^2), \quad (12)
$$

$$
F_{Q^2}^{ab} = \beta^2 \left(\sigma_\Delta^2 - \frac{J^2}{2N} \right), \quad (13)
$$

$$
F_N^a = \beta \left(\Delta_0 - \frac{J_0}{2N} + \frac{\beta J^2}{2} \mu_a + \frac{\beta \sigma_h^2}{2} - \frac{\beta J^2}{4N} + \frac{\beta \sigma_\Delta^2}{2} \right). \quad (14)
$$

Using the saddle point method for $\mathcal{L}$, it is straightforward to verify that

$$
m_a = \langle S^a \rangle, \quad q_{ab} = \langle S^a S^b \rangle, \quad \mu_a = \langle (S^a)^2 \rangle. \quad (15)
$$

To get analytical expressions in the $n \to 0$ limit for these thermal averages with respect to the effective Hamiltonian $\mathcal{H}_{\text{eff}}$, the replica-symmetric (RS) ansatz is used,

$$
m_a = m, \quad q_{ab} = q(1 - \delta_{ab}), \quad \mu_a = \mu. \quad (16)
$$

Then, the single-site normalized weight

$$
P_S = \frac{\exp [\mathcal{H}_{\text{eff}}(\{S^a\})]}{\text{Tr}\{\exp [\mathcal{H}_{\text{eff}}(\{S^a\})]\}} \quad (17)
$$

may be derived to give equations for the relevant order parameters, namely, magnetization m, spin glass q, and concentration μ of ions retaining their magnetic moments (see Supplemental Material [36])

$$
m = \int_z \int_w \frac{2 \sinh [\beta H_S(z)]}{\exp [-\beta H_\Delta(\omega)] + 2 \cosh [\beta H_S(z)]}, \quad (18)
$$

$$
q = \int_z \int_w \frac{4 \sinh^2 [\beta H_S(z)]}{\{\exp [-\beta H_\Delta(\omega)] + 2 \cosh [\beta H_S(z)]\}^2}, \quad (19)
$$

$$
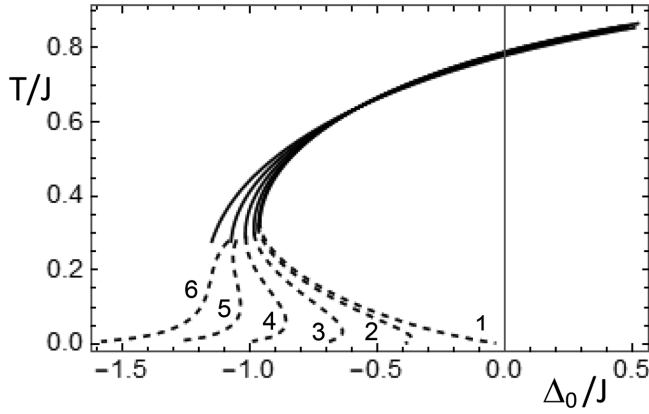\mu = \int_z \int_w \frac{2 \cosh [\beta H_S(z)]}{\exp [-\beta H_\Delta(\omega)] + 2 \cosh [\beta H_S(z)]}. \quad (20)
$$

FIG. 2. Phase diagram as a function of temperature and the parameter Δ_0. The boundary of instability is shown by the solid lines in the replicon sector, and by the broken lines in the anomalous/longitudinal sector. The cases of the ratio σ_Δ/J are taken as (1) 0.0; (2) 0.1; (3) 0.2; (4) 0.3; (5) 0.4; and (6) 0.5.

Here, the shorthand notation is used for integration over the dummy variables z and w

$$\int_{-\infty}^{\infty} \mathcal{D}z \int_{-\infty}^{\infty} \mathcal{D}w = \int_z \int_w,$$

where

$$\mathcal{D}z \equiv \frac{dz}{\sqrt{2\pi}} \exp\left(-\frac{z^2}{2}\right)$$

and a similar expression for ω denotes the measures of integration.

For convenience, the effective fields are introduced here:

$$H_S(z) = h_0 + J_0 m + zJ\sqrt{q + \frac{\sigma_h^2}{J^2}}, \qquad (21)$$

$$H_\Delta(\omega) = \Delta_0 + \frac{\beta J^2}{2}(\mu - q) + \omega\sigma_\Delta. \qquad (22)$$

The equations of the Sherrington-Kirkpatrick (SK) model [37] for m and q are recovered when sending $\Delta_0 \to +\infty$ and $\exp[-\beta H_\Delta(\omega)] \to 0$. In this limit, all intercalated ions are in the high-spin state, and μ is identically 1. In the limit $\sigma_\Delta = 0$, the system (18)–(20) coincides with that of the spin-glass Blume-Emery-Griffiths model (see Eqs. (19)–(21) in Ref. [38]).

B. Stability analysis of RS solutions

Spontaneous fluctuations around replica-symmetric solutions may destroy them. According to the Almeida-Thouless criterion (AT), the RS solution remains stable against fluctuations of the order parameters until all eigenvalues of the Hessian matrix associated with the quadratic Lagrangian of the fluctuations are positive [39]. A detailed calculation of these eigenvalues by means of the replica Fourier transform (RFT) [40,41] and their classification are relegated to the Supplemental Material. The analysis shows the fluctuation space is divided into three sectors, which are identified as the replicon (R), the anomalous (A), and the longitudinal (L).

The instability in the R sector occurs along the AT line given by the condition

$$t^2 = 4 \int_z \int_w \frac{\{\exp[-\beta H_\Delta(\omega)]\cosh[\beta H_S(z)] + 2\}^2}{\{\exp[-\beta H_\Delta(\omega)] + 2\cosh[\beta H_S(z)]\}^4}, \quad (23)$$

where $t = T/J$.

The A and the L sectors yield the same second stability line,

$$\left[t - \frac{J_0}{J}(\mu - q)\right][2t^2 - \mu + K_{\mu\mu}] = \frac{J_0}{J}(K_{m\mu} - m)^2, \quad (24)$$

with

$$K_{\mu\mu} = \int_z \int_w \frac{4\cosh^2[\beta H_S(z)]}{\{\exp[-\beta H_\Delta(\omega)] + 2\cosh[\beta H_S(z)]\}^2},$$

$$K_{m\mu} = \int_z \int_w \frac{4\sinh[\beta H_S(z)]\cosh[\beta H_S(z)]}{\{\exp[-\beta H_\Delta(\omega)] + 2\cosh[\beta H_S(z)]\}^2}.$$

When $J_0 = 0$, the second stability condition (24) is reduced to

$$2t^2 = \mu - K_{\mu\mu}. \qquad (25)$$

Both stability conditions (23) and (24) may be used to determine the effect of the chemical potential Δ_0 and the possibility of singlet ground state paramagnetism, as has been suggested by Ghatak and Sherrington (GS) [34].

In the case of the uniform Δ_0, i.e., when $\sigma_\Delta = 0$, the stability boundary of the paramagnetic phase against fluctuations in the R sector (23) can be recast in the equivalent form [42]

$$\alpha = -\frac{1}{2} + t \ln\left[\frac{t}{2(1-t)}\right], \qquad t \geqslant \frac{1}{3}. \qquad (26)$$

Here, $\alpha = \Delta_0/J$.

The line of stability against fluctuations in the A and the L sectors can be derived from (25) and takes the form

$$\alpha = -\frac{1}{4t}(1 - \sqrt{1 - 8t^2}) + 2t \ln\left[\frac{1 - \sqrt{1 - 8t^2}}{4t}\right] \quad (27)$$

with $t \leqslant 1/3$. The intersection of the two curves (26) and (27) gives the GS tricritical point $t_c = 1/3$ and $\alpha_c = -1/2 - (2/3)\ln 2 \approx -0.962$. Below α_c, i.e., at $\Delta_0 < \alpha_c J$, only the singlet paramagnetic phase is possible.

Nonzero widths σ_Δ shift the tricritical point to the region of lower Δ_0 values (Fig. 2), where the boundaries of instability of the RS solutions against replicon fluctuations coincide with the line of second-order phase transition points as given by Eqs. (10) and (11). Remarkably, the instability lines of the replicon and anomalous/longitudinal sectors cease to intersect at $\sigma_\Delta/J \gtrsim 0.33$. This is in line with the suggestion that the SK ansatz is incapable of locating first-order transition points in spin glasses [42], and their analysis may be done in the full replica symmetry breaking scheme [38,43].

For practical purposes, the dependence of interest is the spin freezing temperature T_f on the average concentration μ of Fe ions retaining their magnetic moments (Fig. 3). It can be obtained from the line separating spin-glass and paramagnetic
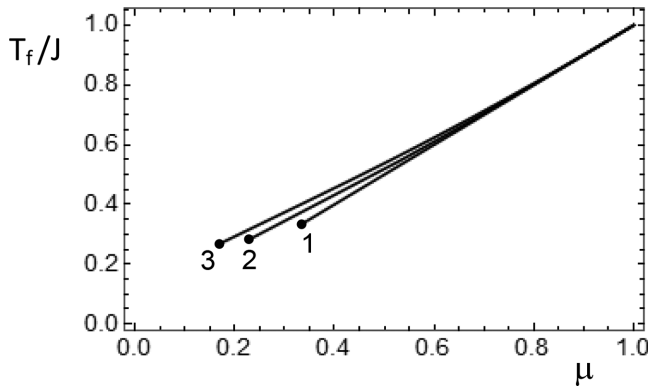
FIG. 3. The zero-field critical frontier T_f/J separating the spin-glass and the singlet paramagnetic phases at $J_0 = 0$ as a function of the average concentration μ of intercalated ions retaining their magnetic moments. The cases of σ_Δ/J are taken: (1) 0.0; (2) 0.3; (3) 0.5. The black dots mark tricritical points.

phases by the softening to zero of the spin-glass parameter q, which results in a pair of the coupled equations

$$\left(\frac{T_f}{J}\right)^2 = \int_w \frac{4}{\{\exp[-\beta_f H_\Delta(\omega)] + 2\}^2}, \tag{28}$$

$$\mu = \int_w \frac{2}{\{\exp[-\beta_f H_\Delta(\omega)] + 2\}} \tag{29}$$

with $H_\Delta(\omega) = \Delta_0 + \frac{1}{2}\beta_f J^2\mu + \omega\sigma_\Delta$ and $\beta_f = 1/T_f$. Here, Δ_0 is treated as a parameter. It can be seen from Fig. 3 that the singlet paramagnetic phase turns out to be stable at small concentrations and T_f scales linearly with μ if the latter exceeds a threshold corresponding to the tricritical point. An increase of σ_Δ just shifts the threshold in the direction of small μ values. The dependence $T_f(\mu)$ demonstrates clearly that the appearance of spin-glass behavior depends crucially on the content of Fe ions in the high-spin state.
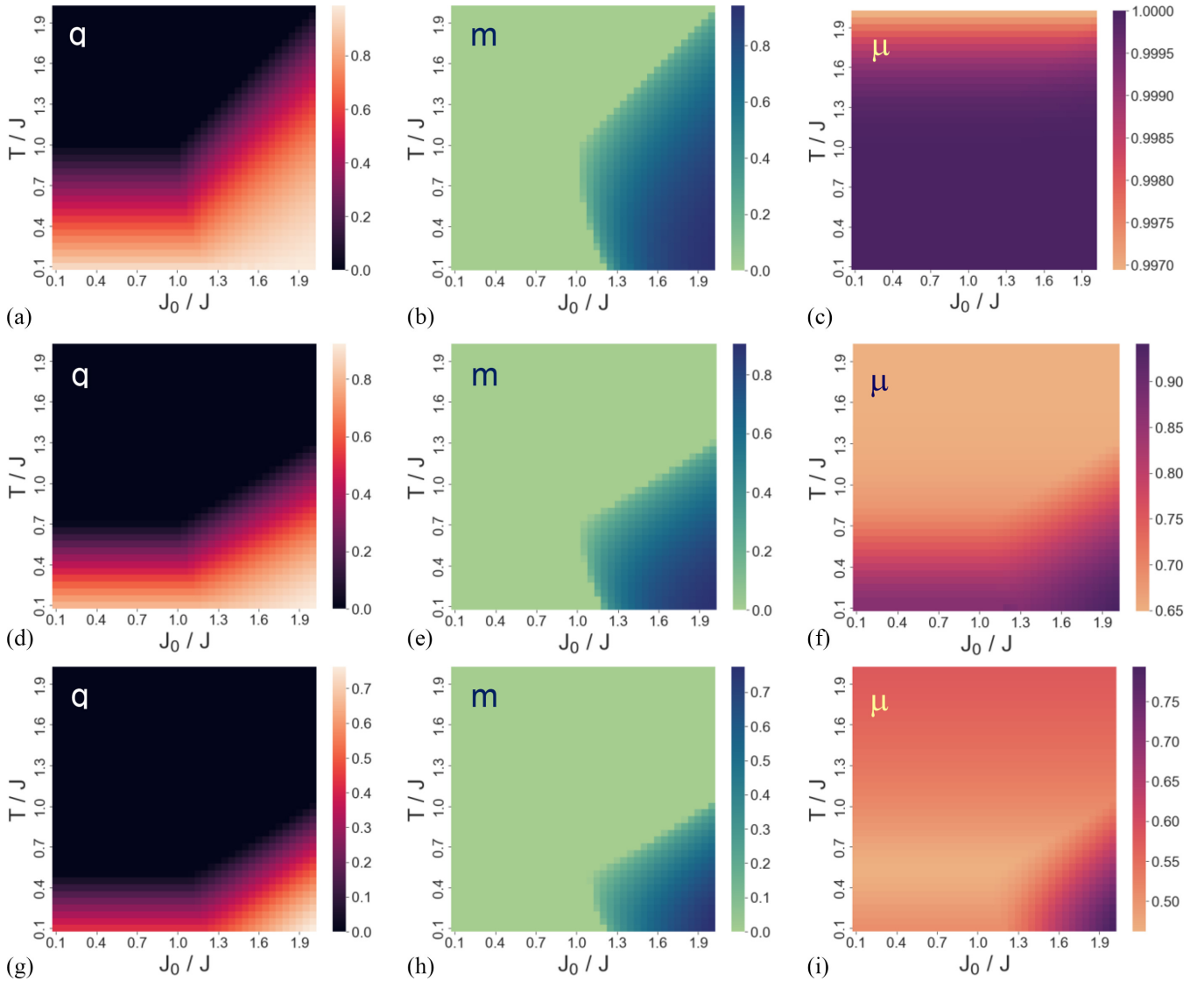

FIG. 4. Plots of the order parameters (the spin glass q, the magnetization μ, and the concentration of magnetically active ions μ) in the absence of random Gaussian fields ($\sigma_h = 0$): (a)–(c) $\Delta_0/J = 10.0$; (d)–(f) $\Delta_0/J = -0.3$; (g)–(i) $\Delta_0/J = -0.9$. Everywhere, $\sigma_\Delta = 0.5$ is taken.
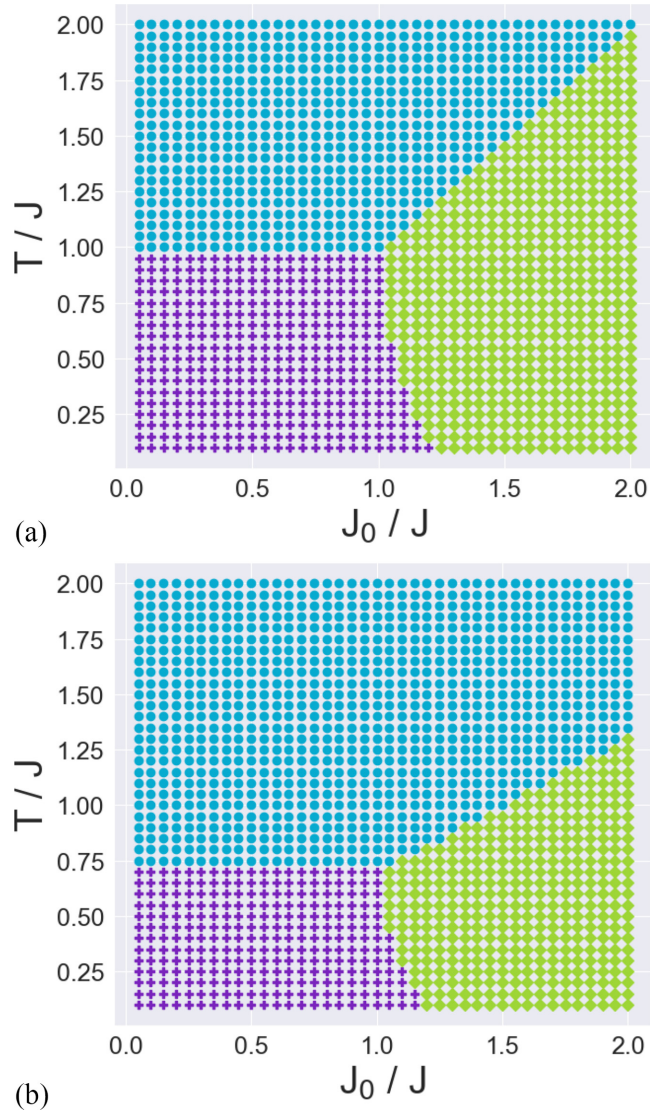
(a)

(b)

FIG. 5. The zero-field ($h_0 = 0$) phase diagrams in the absence of random Gaussian fields ($\sigma_h = 0$): (a) $\Delta_0/J = 10.0$, $\sigma_\Delta = 0.5$; (b) $\Delta_0/J = -0.3$, $\sigma_\Delta = 0.5$. The colors of phases: violet (SG), blue (PM), and green (FM).

C. (J_0/J, T/J)-phase diagrams

A possible appearance of spin-glass ordering at higher concentrations necessitates considering in detail the case of nonzero J_0 when a prevailing distance between the Fe ions arises. Direct calculation of the order parameters, given by Eqs. (18)–(20), provides evidence that no magnetization m occurs for small J_0 values (Fig. 4). This means that the stability relation (26), which determines a position of the tricritical point on the phase diagram, holds. Consequently, we may examine magnetic properties for those Δ_0, which remain higher than that of the tricritical point.

The (J_0/J, T/J)-phase diagrams in the absence of any random fields ($h_0 = 0$, $\sigma_h = 0$) are plotted in Fig. 5. It may be noted that these phase diagrams are similar to that of the SK model. The results indicate the presence of three phases, namely, the spin-glass SG ($m = 0$, $q \neq 0$), the
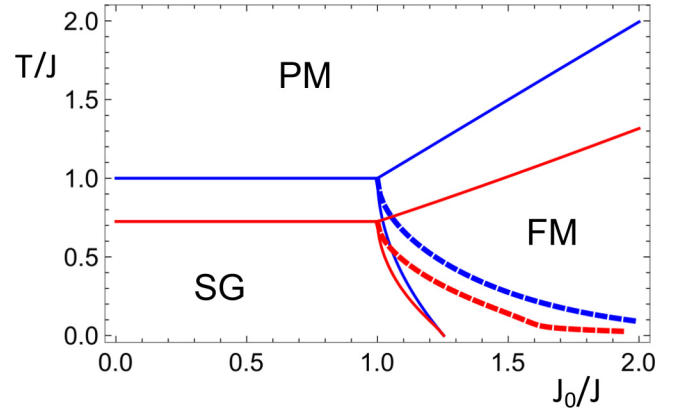

FIG. 6. The phase diagram with the stability line. The PM phase is stable, the SG is entirely unstable, while the FM is only stable over the AT line (dashed). The cases $\Delta_0/J = 10.0$ (blue lines) and $\Delta_0/J = -0.3$ (red lines) are taken. Another parameters are $h_0 = 0$, $\sigma_h = 0$, and $\sigma_\Delta = 0$.

ferromagnetic FM ($m \neq 0$, $q \neq 0$), and the paramagnetic PM ($m = 0$, $q = 0$). The boundary between the SG and PM phases is given by Eqs. (28) and (29). The FM and PM phases are separated by the line $T_c = \mu J_0$, where μ may be found from (29) as well. At last, the FM $\rightarrow$ SG transition is determined by the line $T_m = (\mu - q)J_0$. The order parameters are calculated from Eqs. (19) and (20) with $H_S(z) = zJ\sqrt{q}$. Decreasing of Δ_0 is accompanied by gradual suppression of the magnetically ordered phases.

Numerical evaluation of the stability line (23) on the (J_0/J, T/J)-phase diagram is shown in Fig. 6. As expected, the FM state is unstable at very low temperatures, even at $J_0 > J$, unlike the PM phase, which is always stable. Note that in the limit $\Delta_0 \rightarrow +\infty$ the results of the SK model are recovered. However, when Δ_0 decreases and becomes negative, the instability region tends to be smaller.

Remarkably, the temperature behavior of the concentration μ is drastically modified as Δ_0 decreases, whereas the corresponding evolution of the order parameters q and m demonstrates no qualitative changes [see Fig. 4, panels 4(a), 4(d), 4(g) and Fig. 4, panels 4(b), 4(e), 4(h), respectively]. At large positive Δ_0 values, μ, being close to 1, varies faintly regardless of the phase [Fig. 4(c)]. Further decrease of Δ_0 gives rise to the noticeable difference between the concentration of magnetic ions in the SG phase and that of the FM phase [Fig. 4(f)]. When Δ_0 approaches a value of the tricritical point of the first-order transition to the singlet phase, μ increases in the SG phase with increasing temperature due to thermal activation of the states $S = \pm 1$ [Fig. 4(h)]. In contrast, μ varies with T to a much lesser extent in the FM phase.

D. Effect of random fields

The SK model in the presence of a Gaussian-distributed random magnetic field of mean h_0 and width σ_h has been discussed in Ref. [44]. Our analysis is restricted to the case where $h_0 = 0$, but σ_h is finite. It shows that whenever Δ_0 values prevent the transition to the singlet paramagnetic phase the (J_0/J, T/J)-phase diagrams are analogous to that of the
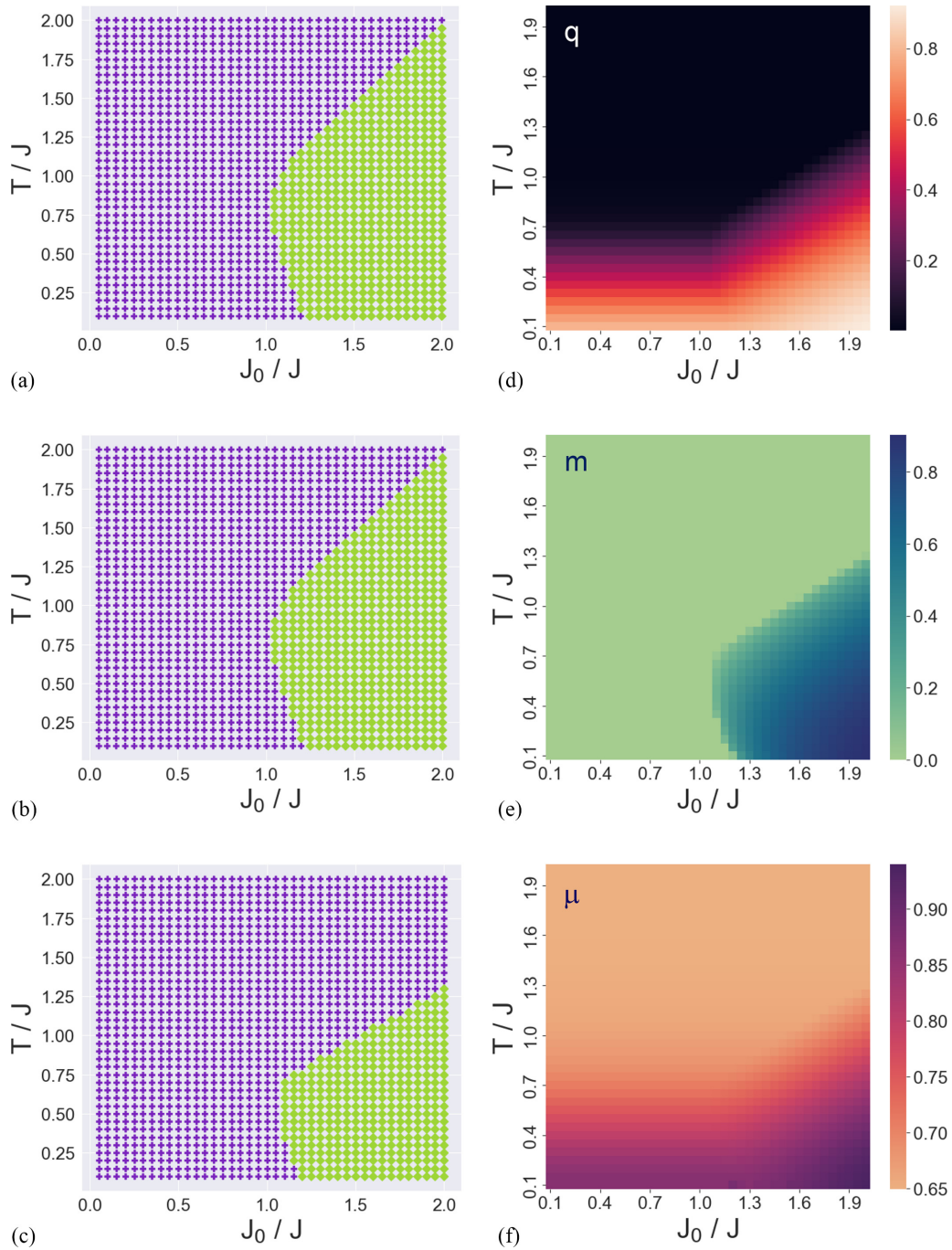
FIG. 7. Zero-field phase diagrams in the presence of random Gaussian fields ($\sigma_h = 0.1$): (a) $\Delta_0/J = 10.0$, $\sigma_\Delta = 0.0$; (b) $\Delta_0/J = 10.0$, $\sigma_\Delta = 0.5$; (c) $\Delta_0/J = -0.3$, $\sigma_\Delta = 0.5$. The I/FM phase is shown by violet/green color. (d)–(f) Plots of the order parameters at $\Delta_0/J = -0.3$, $\sigma_\Delta = 0.5$.

SK model (Fig. 7). Evidently the account of the random fields leads to the disappearance of a clear-cut border between the SG and PM phases as resulted from Eq. (19),

$$q = \int_z \tanh^2\left[\beta z J\sqrt{q + \sigma_h^2/J^2}\right]. \tag{30}$$

Following the classification adopted in Ref. [44] one may identify the *independent* (I) phase ($m = 0$, $q \neq 0$) and the ferromagnetic phase ($m \neq 0$, $q \neq 0$). The frontier between

them is determined by the line

$$T_m = J_0 \int_z \mathrm{sech}^2\left[\beta z J\sqrt{q + \sigma_h^2/J^2}\right]. \tag{31}$$

Detailed information on variation of phase diagrams and concomitant behavior of the order parameters with increase of Δ_0 is presented in the Supplemental Material [36]. Here, it should be emphasized, even though the order parameters behave similarly to the situation where there are no random
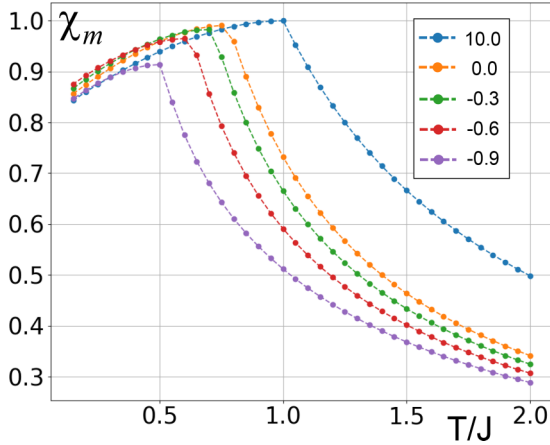
FIG. 8. Magnetic susceptibility without external field for $J_0 = 0.0$ and different values of Δ_0/J shown by figures in the inset. Here, $\sigma_\Delta = 0.0$ and $\sigma_h = 0.0$.

FIG. 9. Evolution of the Almeida-Thouless lines as Δ_0/J varies. The instability region (under the line) is reduced as Δ_0/J decreases: $\Delta_0/J = 10.0$ (black), $\Delta_0/J = 0.0$ (magenta), $\Delta_0/J = -0.3$ (blue), $\Delta_0/J = -0.6$ (red), $\Delta_0/J = -0.9$ (brown).

Weiss fields, the latter tend to support higher concentration of intercalated ions retaining their magnetic moments.

III. MAGNETIC CHARACTERISTICS

A. Magnetic susceptibility

Next, we address the magnetic susceptibility. First, we note that all three order parameters m, q, and μ depend on the magnetic field h_0, and three related independent susceptibilities should be therefore defined,

$$\chi_m = \frac{\partial m}{\partial h_0}, \quad \chi_q = \frac{\partial q}{\partial h_0}, \quad \chi_\mu = \frac{\partial \mu}{\partial h_0}. \quad (32)$$

The relationship between these quantities is established through the coupled set of linear equations

$$\begin{pmatrix} 1 - \beta J_0(\mu - q) & \beta^2 J^2 I_1 - \beta J I_2 \lambda & -\beta^2 J^2 I_1 \\ -\beta J_0 I_3 & 1 - \beta J I_4 \lambda + \beta^2 J^2 I_5 & -\beta^2 J^2 I_5 \\ -\beta J_0(m - I_7) & \beta^2 J^2 I_8 - \beta J I_6 \lambda & 1 - \beta^2 J^2 I_8 \end{pmatrix}$$

$$\times \begin{pmatrix} \chi_m \\ \chi_q \\ \chi_\mu \end{pmatrix} = \begin{pmatrix} \beta(\mu - q) \\ \beta I_3 \\ 2\beta I_1 \end{pmatrix} \quad (33)$$

in which the coefficients contain the integrals I_k ($k = 1, \ldots, 8$) listed in the Appendix, and $\lambda = 1/\sqrt{q + \sigma_h^2/J^2}$.

Zero-field susceptibilities for different values of Δ_0 are plotted in Fig. 8, when distribution of the exchange couplings is centered around zero. The spin freezing temperature is marked by a cusp in the susceptibility, which adopts the Curie form above T_f. The cusp temperature is shifted closer to zero with a decrease of Δ_0.

Turning to the limit $\Delta_0 \to \infty$, when $I_{1,2} = 0$ and $\mu = 1$, the result of the SK model is recovered from (33)

$$\chi_m = \frac{\beta(1 - q)}{1 - \beta J_0(1 - q)}. \quad (34)$$

Behavior of magnetic susceptibility in finite magnetic fields may be used for experimental verification of the BC
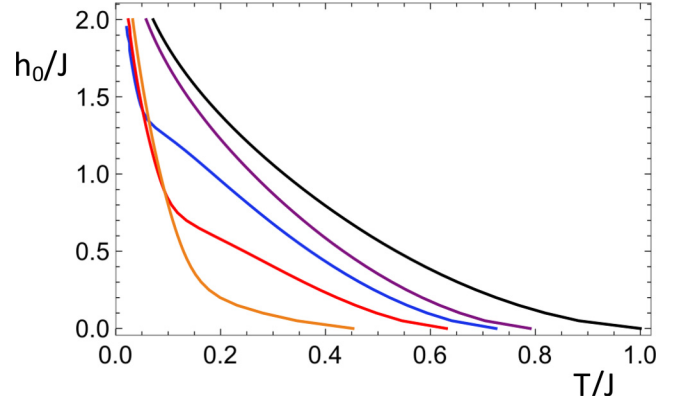
model. Increasing of the field h_0 facilitates stability of the RS solution as evident from Fig. 9, where the AT lines are plotted at different Δ_0/J values for the case in which J_0 is zero. It is seen that a decrease of the chemical potential Δ_0 leads to enlargement of the region of stability of the RS solution.

Figure 10 summarizes the behavior of the susceptibility at finite magnetic fields and in the presence of the random Weiss fields. Once the external field h_0 is applied, the cusp in the zero-field susceptibility is rounded off and the χ curves go upward with further increase of h_0 during a cooling process. Simultaneously, the increase of the field leads to the appearance of a broad peak at temperatures above T_f, which tends to be more pronounced at finite J_0 [Fig. 10, panels 10(b), 10(d), 10(f)]. This effect is related to increase of a fraction μ of the intercalated ions retaining their magnetic moments under the action of the field. The secondary broad peak shifts to lower temperatures when the chemical potential Δ_0 decreases, since its position is controlled by the precipitous fall of Curie-law susceptibility above the freezing temperature, which is reduced with decreasing of μ (see Fig. 3).

B. Magnetization

Finally, we mention how the chemical potential Δ_0 alters the magnetization process (Fig. 11). For large positive values of Δ_0, when our model is closely analogous to the standard SK model, the magnetization curves, which are far from saturation, have practically temperature-independent slope [Fig. 11(a)]. However, smaller values of Δ_0 lead to steepening of magnetization curves when temperature increases [Fig. 11(b)]. Similar to the temperature dependence of magnetic susceptibility in finite magnetic fields, the reason for this is related to faster destroying of spin-glass order upon heating, which may suppress competing growth of magnetization due to thermal activation of high-spin states of the Fe-doped ions.

C. How to vary Δ_0 in the related compounds

The appearance of spin-glass behavior in the BC model with the Hamiltonian (1) is controlled by the parameters Δ_i.
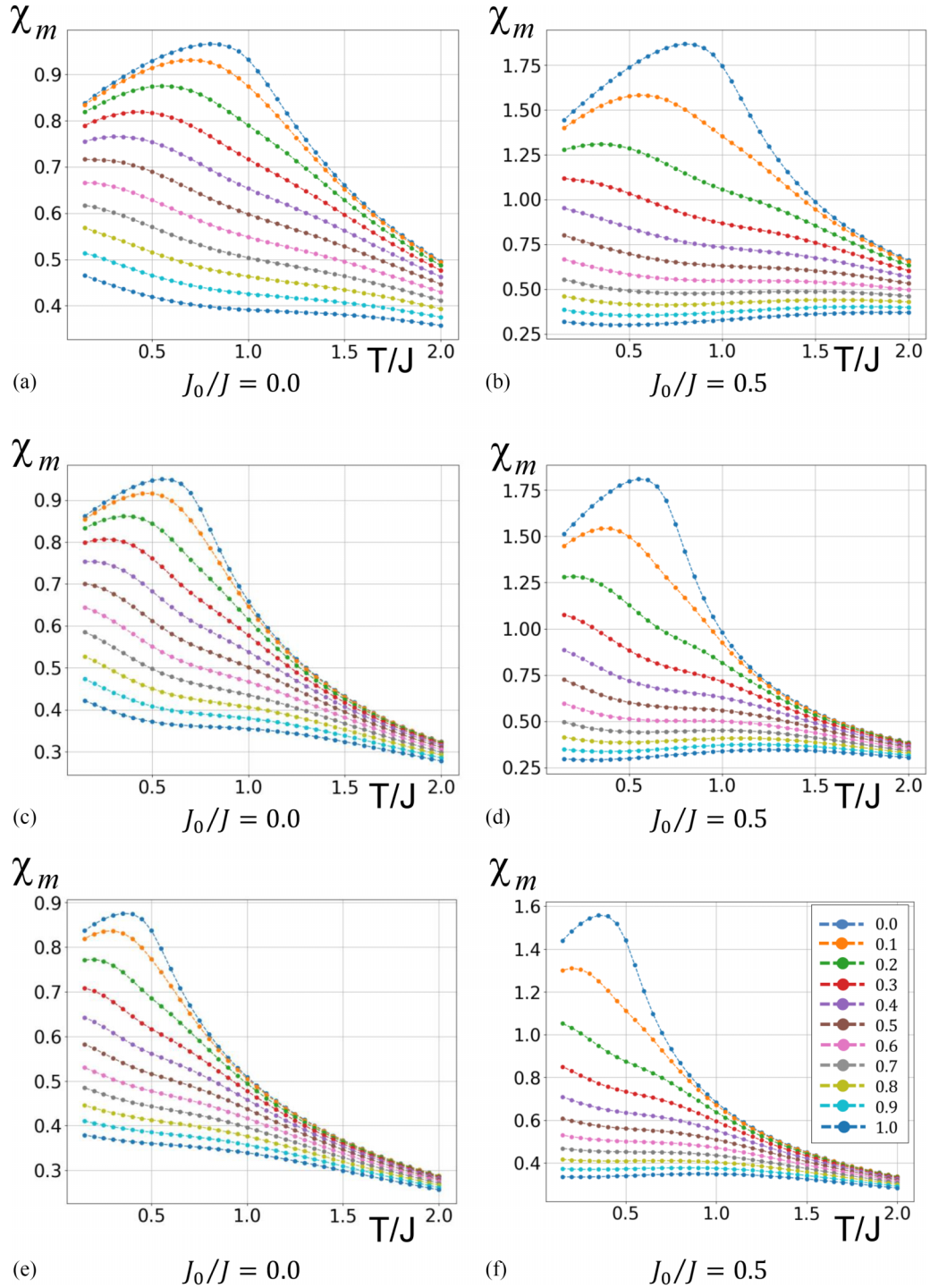
FIG. 10. Evolution of temperature dependence of the susceptibility with an external magnetic field h_0/J marked by colors in the inset of the plot (f): (a), (b) $\Delta_0/J = 10.0$; (c), (d) $\Delta_0/J = -0.3$; (e), (f) $\Delta_0/J = -0.9$. Here, $\sigma_\Delta = 0.5$ and $\sigma_h = 0.1$.

In the previous theoretical studies of the BC spin-glass model, the uniform parameter $\Delta = \Delta_i$ was attributed either to crystal field energy [34] or to anisotropy energy in the $S - 1$ Ising model [42]. In our case of the normally distributed Δ_i with the mean Δ_0, the latter determines whether the fraction μ of Fe ions inserted into the vdW gaps is sufficient or not to maintain spin-glass ordering (see Fig. 3). Therefore, we may suggest that in the systems where spin-glass effects

are manifested ($2H$-Fe$_x$TaSe$_2$, $4Hb$-Fe$_x$TaS$_2$), μ exceeds a threshold value, while it is lower than the critical value in the materials ($2H$-Fe$_x$TaS$_2$, $4Hb$-Fe$_x$TaSe$_2$) exhibiting singlet ground state paramagnetism with embedded magnetic impurities. Note, although an increase of the Gaussian distribution width σ_Δ diminishes the threshold of μ, it is highly unlikely that this intrinsic parameter may be modified in a controllable manner.
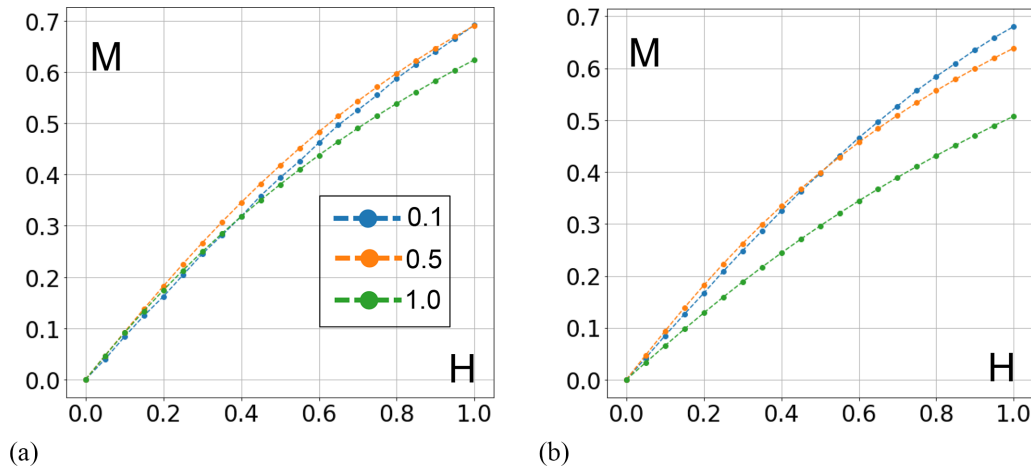
FIG. 11. Magnetization curves for $\Delta_0/J = 10.0$ (a) and $\Delta_0/J = -0.3$ (b). The inset: The plot colors are marked by figures of temperature T/J. The parameters $J_0/J = 0$, $\sigma_\Delta = 0.5$, and $\sigma_h = 0.1$ are taken in all cases.

At present, it is widely recognized that co-intercalation provides a powerful and feasible tool for tuning magnetic properties of transition metal dichalcogenides [45–48]. In view of the alternative, we propose a way to verify validity of the BC model for describing spin-glass effects in the Fe-doped $TaS_2(Se_2)$ compounds by means of co-intercalation of non-Kramers $3d$ ions into the vdW gaps. In ions with an even number of electrons in the $3d$ shell, singlet ground-state levels may result under low crystalline symmetry; however, this is not the case for the non-Kramers ions with odd number of electrons in the respective shell. As a result, their co-doping increases a total proportion of intercalated ions retaining their magnetic moments.

Indeed, let μN be the initial number of such Fe ions, where N is a total number of the doped iron elements including those whose moments are lost. Addition of the n non-Kramers ions changes the balance to

$$\mu_{\text{eff}} = \frac{\mu N + n}{N + n} = \mu + (1 - \mu)\frac{n}{n + N}. \tag{35}$$

Since $\mu_{\text{eff}} > \mu$, it may exceed a threshold value necessary to support spin-glass ordering in the system. Therefore, the co-doped non-Kramers ions may trigger a spin-glass regime in the materials with the initial singlet paramagnetic phase.

Obviously, properties of the doping-induced SG phase cannot be unambiguously attributed to the co-intercalated ions only. This concentration mismatch will be a hallmark of the Blume-Capel model relevance.

IV. CONCLUSIONS

Our study is aimed to explain why Fe intercalation into the layered $TaS_2(Se_2)$ polytypes brings spin-glass behavior in one group of these complexes, while another group tends to be nonmagnetic. We propose an explanation of the problem based on the spin-glass Blume-Capel model. Besides the usual exchange coupling, the model includes normally distributed random one-site potentials, which govern magnetic states of the intercalated Fe ions. A mean of the distribution

Δ_0 regulates the balance between those Fe ions that lose their magnetic moments and those that retain them.

The Ghatak-Sherrington theory predicts the existence of a tricritical point, in which the line of the second-order phase transition to the SG state breaks, when plotted versus Δ_0, and the system undergoes a sharp transition to the singlet paramagnetic state. When a number of the intercalated Fe ions in the high-spin state exceeds a threshold value, which is determined by the tricritical point, spin-glass ordering may occur. This fact provides a plausible explanation for division into nonmagnetic and spin-glass systems observed in the family of the Fe-doped $TaS_2(Se_2)$ crystals.

Properties of the spin-glass behavior described by the BC model differ little from that of predicted by the Sherrington-Kirkpatrick model with fixed number of magnetic ions. Nonetheless, we note characteristic features in the temperature dependence of paramagnetic susceptibility and in the field dependence of magnetization, which could confirm the relevance of the BC model for the materials of interest. The appearance of these specific features is due to the fact that a certain portion of Fe ions in the low-spin state may regain their magnetic moments on heating or under the influence of an external magnetic field.

The unique crystal structure of the layered vdW transition metal dichalcogenides makes it possible to increase a content of ions with magnetic moments through insertion of non-Kramers $3d$ ions into the vdW gap. These co-intercalant elements may trigger the spin-glass phase in the initially nonmagnetic Fe-doped $TaS_2(Se_2)$ complexes. A distinguishing feature of the doped-induced SG ordering is that the corresponding concentration of magnetic ions will comprise not only the co-intercalant elements, but also Fe ions in the high-spin state. This concentration mismatch to the content of the doped non-Kramers $3d$ ions can be used for independent verification of the BC spin-glass model.

APPENDIX: INTEGRALS FOR MAGNETIC SUSCEPTIBILITY

Here is a list of integrals involved in calculation of the magnetic susceptibility χ_m:

$$I_1 = \int_z \int_w \frac{\sinh[\beta H_S(z)] \exp[-\beta H_\Delta(\omega)]}{\{\exp[-\beta H_\Delta(\omega)] + 2\cosh[\beta H_S(z)]\}^2},$$

$$I_2 = \int_z \int_w \frac{z\{\exp[-\beta H_\Delta(\omega)]\cosh[\beta H_S(z)] + 2\}}{\{\exp[-\beta H_\Delta(\omega)] + 2\cosh[\beta H_S(z)]\}^2},$$

$$I_3 = \int_z \int_w \frac{\{\exp[-\beta H_\Delta(\omega)]\cosh[\beta H_S(z)] + 2\}}{\{\exp[-\beta H_\Delta(\omega)] + 2\cosh[\beta H_S(z)]\}^3}$$
$$\times 8\sinh[\beta H_S(z)],$$

$$I_4 = \int_z \int_w \frac{\{\exp[-\beta H_\Delta(\omega)]\cosh[\beta H_S(z)] + 2\}}{\{\exp[-\beta H_\Delta(\omega)] + 2\cosh[\beta H_S(z)]\}^3}$$
$$\times 4z\sinh[\beta H_S(z)],$$

$$I_5 = \int_z \int_w \frac{4\sinh^2[\beta H_S(z)]\exp[-\beta H_\Delta(\omega)]}{\{\exp[-\beta H_\Delta(\omega)] + 2\cosh[\beta H_S(z)]\}^3},$$

$$I_6 = \int_z \int_w \frac{z\sinh[\beta H_S(z)]\exp[-\beta H_\Delta(\omega)]}{\{\exp[-\beta H_\Delta(\omega)] + 2\cosh[\beta H_S(z)]\}^2},$$

$$I_7 = \int_z \int_w \frac{4\sinh[\beta H_S(z)]\cosh[\beta H_S(z)]}{\{\exp[-\beta H_\Delta(\omega)] + 2\cosh[\beta H_S(z)]\}^2},$$

$$I_8 = \int_z \int_w \frac{\cosh[\beta H_S(z)]\exp[-\beta H_\Delta(\omega)]}{\{\exp[-\beta H_\Delta(\omega)] + 2\cosh[\beta H_S(z)]\}^2}. \quad (A1)$$

[1] J. A. Wilson and A. D. Yoffe, Adv. Phys. **18**, 193 (1969).

[2] V. L. Kalikhman and Ya. S. Umanskii, Sov. Phys. Usp. **15**, 728 (1973).

[3] A. A. Tedstone, P. J. Lewis, and P. O'Brien, Chem. Mater. **28**, 1965 (2016).

[4] B. Zhao, D. Y. Shen, Z. C. Zhang, P. Lu, M. Hossain, J. Li, B. Li, and X. D. Duan, Adv. Funct. Mater. **31**, 2105132 (2021).

[5] M. Rajapakse, B. Karki, U. O. Abu, S. Pishgar, M. R. K. Musa, S. M. Shah Riyadh, M. Yu, G. Sumanasekera, and J. B. Jasinski, npj 2D Mater. Appl. **5**, 30 (2021).

[6] E. A. Marseglia, Int. Rev. Phys. Chem. **3**, 177 (1983).

[7] G. H. Han, D. L. Duong, D. H. Keum, S. J. Yum, and Y. H. Lee, Chem. Rev. **118**, 6297 (2018).

[8] A. D. Yoffe, in *Physics and Chemistry of Electrons and Ions in Condensed Matter*, edited by J. V. Acrivos, N. F. Mott, and A. D. Yoffe (Springer, Dordrecht, 1984), NATO ASI Series Vol. 130.

[9] S. S. P. Parkin and R. H. Friend, Philos. Mag. B **41**, 65 (1980).

[10] M. Inoue, H. P. Hughes, and A. D. Yoffe, Adv. Phys. **38**, 565 (1989).

[11] V. G. Pleschov, N. V. Baranov, A. N. Titov, K. Inoue, M. I. Bartashevich, and T. Goto, J. Alloys Compd. **320**, 13 (2001).

[12] V. I. Maksimov, N. V. Baranov, V. G. Pleschov, and K. Inoue, J. Alloys Compd. **384**, 33 (2004).

[13] L. J. Li, W. J. Lu, X. D. Zhu, X. B. Zhu, Z. R. Yang, W. H. Song, and Y. P. Sun, J. Magn. Magn. Mater. **323**, 2536 (2011).

[14] N. M. Toporova, E. M. Sherokalova, N. V. Selezneva, V. V. Ogloblichev, and N. V. Baranov, J. Alloys Compd. **848**, 156534 (2020).

[15] H. Nobukane, Y. Tabata, T. Kurosawa, D. Sakabe, and S. Tanda, J. Phys.: Condens. Matter **32**, 165803 (2020).

[16] T. Yoshioka and Y. Tazuke, J. Phys. Soc. Jpn. **54**, 2088 (1985).

[17] Y. Tazuke, T. Yoshioka, and K. Hoshi, J. Magn. Magn. Mater. **54**, 73 (1986).

[18] Y. Tazuke, T. Saitoh, F. Matsukura, T. Satoh, T. Miyadai, and K. Hoshi, J. Phys. Colloques **49**, C8-1507 (1988).

[19] M. Koyano, M. Suezawa, H. Watanabe, and M. Inoue, J. Phys. Soc. Jpn. **63**, 1114 (1994).

[20] Y. Kuroiwa, M. Nishimura, R. Nakajima, H. Abe, and Y. Noda, J. Phys. Soc. Jpn. **63**, 4278 (1994).

[21] D. R. Huntley, M. J. Sienko, and K. Hiebl, J. Solid State Chem. **52**, 233 (1984).

[22] H. Negishi, A. Shoube, H. Takahashi, Y. Ueda, M. Sasaki, and M. Inoue, J. Magn. Magn. Mater. **67**, 179 (1987).

[23] N. V. Selezneva, N. V. Baranov, E. M. Sherokalova, A. S. Volegov, and A. A. Sherstobitov, Phys. Rev. B **104**, 064411 (2021).

[24] N. V. Selezneva, E. M. Sherokalova, A. Podlesnyak, M. Frontzek, and N. V. Baranov, Phys. Rev. Mater. **7**, 014401 (2023).

[25] J. Choe, K. Lee, C.-L. Huang, N. Trivedi, and E. Morosan, Phys. Rev. B **99**, 064420 (2019).

[26] T. Kanno, T. Matsumoto, K. Ichimura, T. Matsuura, and S. Tanda, J. Low Temp. Phys. **183**, 41 (2016).

[27] S. J. Hillenius, R. V. Coleman, E. R. Domb, and D. J. Sellmyer, Phys. Rev. B **19**, 4711 (1979).

[28] M. Eibschütz and F. J. Di Salvo, Phys. Rev. Lett. **36**, 104 (1976).

[29] F. J. Di Salvo and J. V. Waszczak, J. Phys. Colloques **37**, C4-157 (1976).

[30] M. Eibschütz, M. E. Lines, and F. J. Di Salvo, Phys. Rev. B **15**, 103 (1977).

[31] K.-T. Ko, K. Kim, S. B. Kim, H.-D. Kim, J.-Y. Kim, B. I. Min, J.-H. Park, F.-H. Chang, H.-J. Lin, A. Tanaka, and S.-W. Cheong, Phys. Rev. Lett. **107**, 247201 (2011).

[32] M. Blume, Phys. Rev. **141**, 517 (1966).

[33] H. W. Capel, Physica **32**, 966 (1966).

[34] S. K. Ghatak and D. Sherrington, J. Phys. C **10**, 3149 (1977).

[35] M. Blume, V. J. Emery, and R. B. Griffiths, Phys. Rev. A **4**, 1071 (1971).

[36] See Supplemental Material at http://link.aps.org/supplemental/10.1103/PhysRevB.109.054403 for replica technique and phase diagrams in the presence of random Weiss fields.

[37] D. Sherrington and S. Kirkpatrick, Phys. Rev. Lett. **35**, 1792 (1975).

[38] A. Crisanti and L. Leuzzi, Phys. Rev. B **70**, 014409 (2004).

[39] J. R. L. de Almeida and D. J. Thouless, J. Phys. A: Math. Gen. **11**, 983 (1978).

[40] C. De Dominicis and I. Giardina, *Random Fields and Spin Glasses: A Field Theory Approach* (Cambridge University Press, New York, 2006).

[41] I. R. Pimentel and C. De Dominicis, J. Phys. A: Math. Theor. **47**, 455001 (2014).

[42] E. J. S. Lage and J. R. L. de Almeida, J. Phys. C **15**, L1187 (1982).

[43] A. Crisanti and L. Leuzzi, Phys. Rev. Lett. **89**, 237204 (2002).

[44] R. F. Soares, F. D. Nobre, and J. R. L. de Almeida, Phys. Rev. B **50**, 6151 (1994).

[45] M. Inoue, M. Koyano, H. Negishi, and M. Sasaki, Mol. Cryst. Liq. Cryst. Sci. Technol. Sect. A **245**, 37 (1994).

[46] S. Pan, L. Tang, Y. Bai, J. Tang, Z. Zhang, B. Chen, Y. Guo, J. Zhu, G. Xu, and F. Xu, Phys. Rev. Mater. **7**, 034407 (2023).

[47] H. Chen, S. Li, S. Huang, L. Ma, S. Liu, F. Tang, Y. Fang, and P. Dai, Acta Mater. **222**, 117438 (2022).

[48] S. Tang, P. Li, H. Dong, B. Chen, Z. Huang, and H. Tang, J. Electron. Mater. **52**, 7614 (2023).